Cell Type Diversity in the Norepinephrine Signaling Network

By

Amelia Culp

Presented to the Neuroscience Graduate Program
at the Oregon Health and Science University
School of Medicine
In partial fulfillment of
the requirements for the degree of:
Master of Science in Neuroscience

March 2023

Table of Contents

Abstract:

Norepinephrine (NE) is a neuromodulator that alters processing in nearly every brain area, leading to dynamic changes in behavior. NE plays a vital role in arousal, attention, stress, and memory formation through widespread neuronal projections. The transmitter release from these processes allows cells in the network to contribute to diverse behavioral outcomes. The locus coeruleus (LC), a small nucleus in the brainstem's pons, is the canonical source of NE to the forebrain and was traditionally studied as a homogenous unit[1]. However, some studies suggest that non-LC NE projections are present in many brain regions and originate from developmentally distinct groups of cells adjacent to LC.[2–4] Furthermore, recent evidence has challenged the traditional view that LC acts as a uniform output. Rather, both LC and non-LC NE projection cells are organized into functionally heterogeneous groups.[5] These pieces of evidence suggest that the NE system mediates diverse outcomes through a modular architecture composed of functionally distinct groups of cells. However, the full mechanistic explanation of this functional heterogeneity is still unknown.[6] In what follows, I will discuss the historical development of the NE research field, building to a picture of the modern view of diverse NE cell types within and around the LC. I will further document the experimental efforts by myself and my colleagues over the last two years toward elucidating this diversity of cellular function in the NE signaling network.

Chapter 1: Introduction & Background:

1.1 Discovery of catecholamines

The discovery and early study of NE as a neurotransmitter was predicated upon its chemical identity as a catecholamine, one of a family of neuro-hormones that includes dopamine (DA), epinephrine (EPI), and NE.[7] EPI, or adrenaline, was the first catecholamine to be studied when it was identified in 1895 as an adrenal extract and found to have dramatic biological effects following intravenous injection.[8] It was also the first catecholamine to be identified in brain tissue in the 1940s,[9] followed shortly by similar isolation from brain tissue of its chemical precursors, DA and NE.

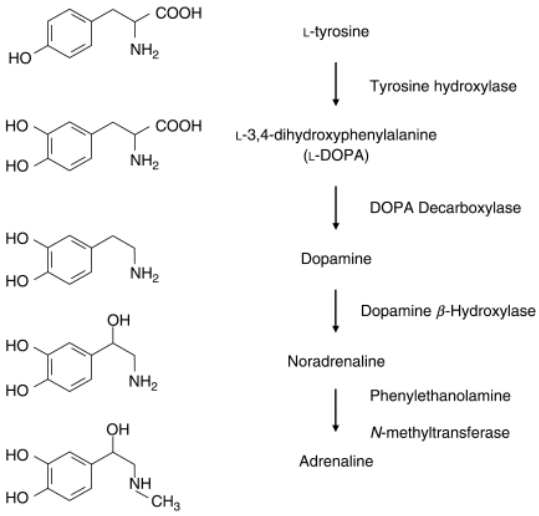

Figure 1.1 The adrenaline synthesis pathway.[10] Chemical precursors to NE are pictured including DA, as well as critical enzymes tyrosine hydroxylase (TH) and Dopamine β-Hydroxylase (Dbh).

The significance of NE's chemical relationship to other catecholamines extends beyond the circumstance of its discovery. Because EPI, NE, and DA are produced along the same synthesis pathway (Fig 1.1[10]), they are present in many of the same cells (DA and NE can be found in all EPI cells and DA in all NE cells, along with the requisite enzymes for each step in the chemical conversion). As such, they are involved in many of the same signaling networks in the brain. Furthermore, NE and EPI activate many of the same adrenoceptors on post-synaptic cells. The precise overlap and/or interaction of catecholamine functions, though, largely remains to be delineated.

1.2 Morphological sub-types

As a first pass, NE cells can be divided into types by their soma morphology. This division of morphological types has been quantitatively undertaken and described in detail in a 1986 study by Loughlin, Foote, and Grzanna[1]. They found that NE cells can be divided into four distinct topo-morphological types based on soma location and shape. They named these types 'Core,' 'Fusiform,' 'Multipolar,' and 'Posterior Pole' cells, as illustrated in Figure 1.2. The authors of this study mapped the efferent projections of each topo-morphological type by injecting the retrograde tracing agent horseradish-peroxidase (HRP) in terminal fields in a selection of candidate projection regions. In doing so, they found distinct projection profiles between each topo-morphological category, represented by bar plots in Figure 1.2 B.

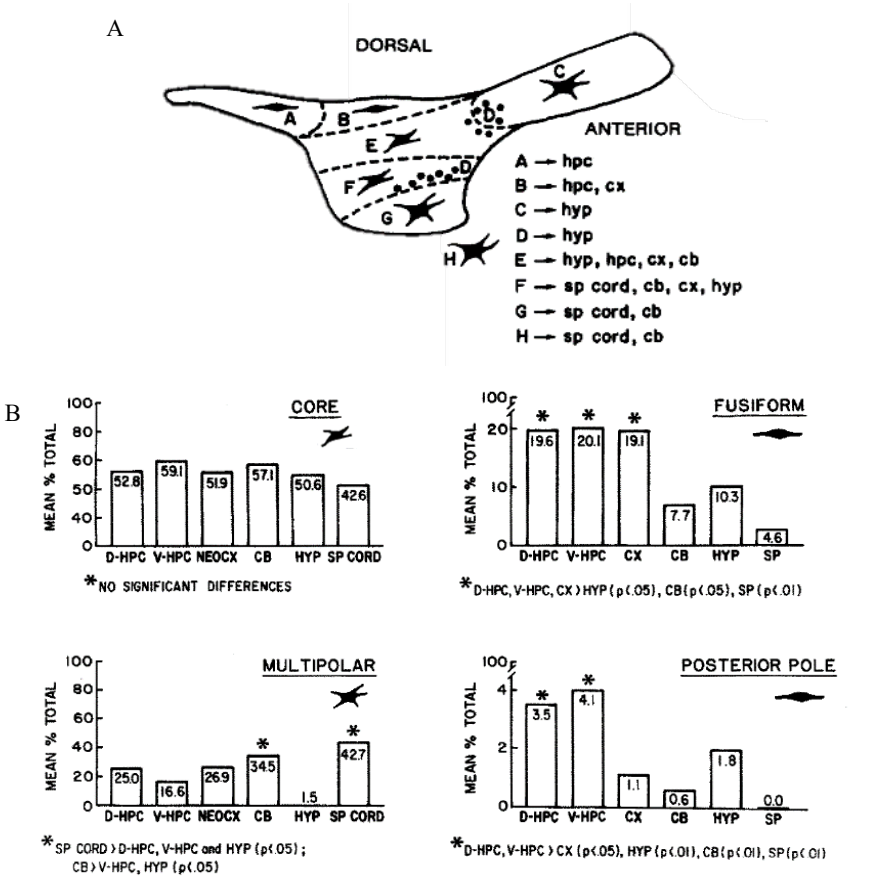

Figure 1.2 Classical findings show differential projection patterns by LC morphological type. (A) Projection groups A-H are spatially modularized and morphologically distinct. (B) Quantification of each topo-morphological type's contribution to total LC projections by target area CB, cerebellum; CX, cortex; D-HPC, V-HPC; dorsal, ventral hippocampus; HYP, hypothalamus, SP CORD, spinal cord. Adapted from[1]

1.3 Afferent connectivity

Part of the early efforts to elucidate the role of NE in the brain included tracing studies that mapped the inputs to NE cells from central and peripheral targets. Since NE-producing cells are so tightly localized in the midbrain, this type of study could be readily accomplished with retrograde tracers and degeneration studies. Initial findings were presented by G.V. Russell in the 1950s[11], which were followed by a flood of studies in the 1960s and 70s by R.S. Snider[12], A. Schiebel[13], N. Shimizu[14,15], and others.

The most comprehensive of the afferent tracing studies from this period, however, were undertaken by Cedarbaum and Aghajanian and published in the Journal of Comparative

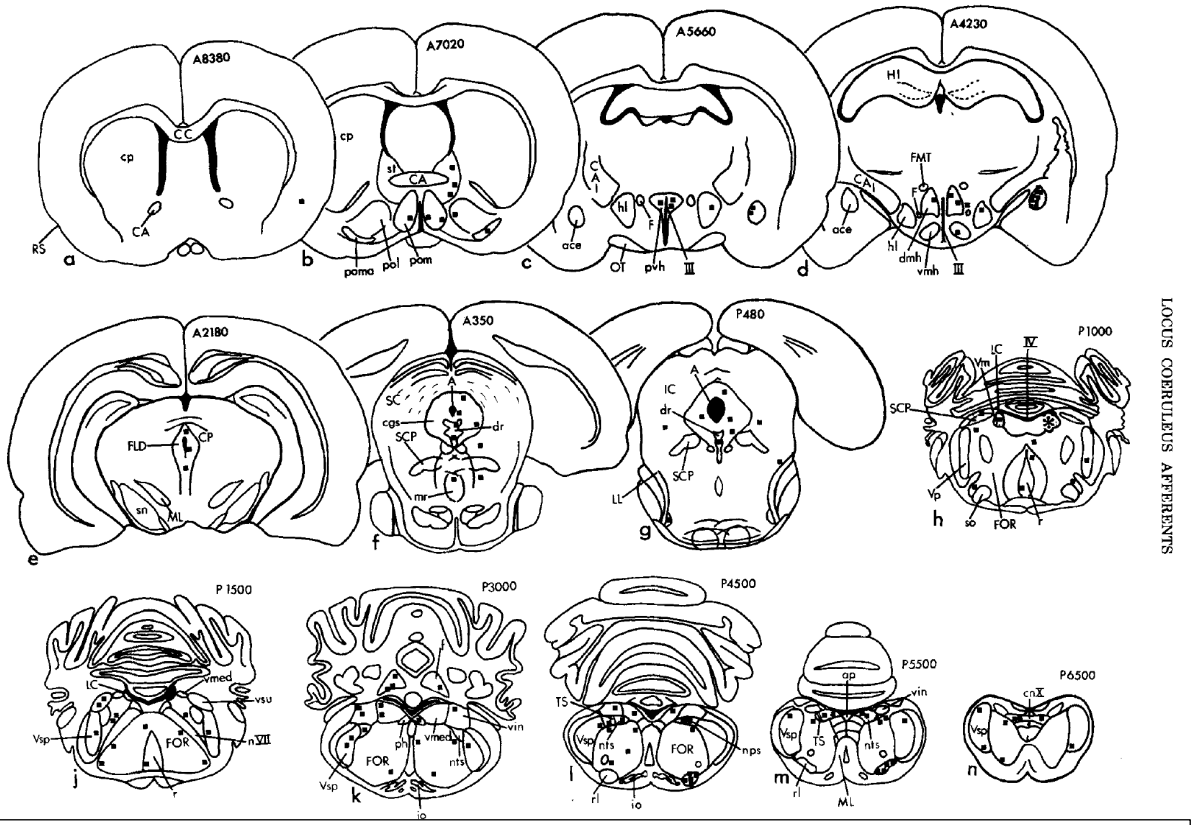

Figure 1.3: LC afferents drawn from representative transverse sections of the rat brain showing locations of reactive cells following HRP injection in LC.[10] A, aqueduct of sylvius; ace, central amygdala; ap, area postrema; CA, anterior commissure; CAI internal capsule; CC, corpus callosum; cgs, central grey; cn commissural nucleus; F, fornix; f, fastigial nucleus; FLD, dorsal longitudinal fasciculusl FMT, mammillothalamic tract; FOR, reticular formation; FR, fasciculus retrflexus; HI, hippocampus; hl, lateral hypothalamus; IC, inferior colliculus; io, inferior olive; lc, locus coeruleus; LL, lateral lemniscus; MFB, medial forebrain bundle; ML, medial lemniscus; nps, nucleus parasolitarius; nts, nucleus tractus solitarius; nVII, cranial nerve VII; OT, optic tract; pf, parafascicular nucleus; ph, nucleus prepositus; pol, lateral preoptic nucleus; pom, medial preoptic nucleus; poma, magnocellular preoptic nucleus; pvh, paraventricular hypothalamus; RS, rhinal sulcus; rl, lateral reticular nucleus; vmh, ventromedial hypothalamus

Neurology in 1978.[16] Similar to the morpho-anatomical experiments conducted by Loughlin and colleagues, this study also used HRP, this time injected into the LC of rodents to trace incoming connections from the brain and spinal cord. They identified 17 distinct input areas in the forebrain including the insular cortex, the central nucleus of the amygdala, preoptic areas, the bed nucleus of the stria terminalis, and hypothalamic areas. Additionally, they found inputs from the brainstem including the central grey, the reticular formation, the raphe, vestibular, solitary tract and lateral reticular nuclei. Importantly, this study documented local connectivity to the LC from nearby NE cell groups in catecholamine areas A_1, A_2, and A_5. Lastly, fastigial nuclei and the marginal zones of the dorsal horns of the spinal cord also contained reactive cells indicating LC input. These afferent input areas are summarized in Figure 1.3.

One afferent area, in particular, was the source of some disagreement during this period: following Cedarbaum and Aghajanian's report of afferent connectivity from the central amygdala (CeA) to the LC, two studies that focused on efferent outputs of the CeA expressly reported no connectivity to LC. Krettek & Price in 1978[17] and Post & Mai in 1980[18] both used light microscopic autoradiography to trace outgoing fibers from CeA and found no label in LC.

The following year, R.M. Clavier published another study documenting LC afferent connectivity, finding primarily subcortical structures in the pons, thalamus, periaqueductal grey, and contralateral LC that provided afferent innervation to the LC.[19] Clavier did not provide a negative or positive report on LC connectivity from CeA, but later studies including J.L. Price's own 1981 paper[20] and modern studies including a comprehensive viral-genetic mapping of LC inputs from 2015[21] have confirmed CeA's axonal connection to LC.

1.4 Efferent projections

Classical anatomy studies defining the distribution of axonal outputs from NE cells were undertaken throughout the 1970s, 80s, and 90s, focusing primarily on LC-NE cells, as non-LC cells containing NE were generally considered to have only limited projections to the forebrain.[22]

The earliest projection studies described outgoing fiber tracts in qualitative strokes, but even in the early 70's it was apparent that ascending NE fibers diverge into two major pathways. Maeda and Shimizu called these pathways the "coerulo-cortical system and the ponto-hypothalamic system," claiming that the first had been previously described by several Swedish groups who had published NE studies in the previous couple of years,[23] but that the second was novel and could be considered "intermediate noradrenergic beam."[15] In notable contrast to the morphology studies of the 1980s described in section 1.2, Maeda and Shimizu claimed that "There is no topographic subdivision of the main part of the locus coeruleus and it appears that a single neuron can innervate all cortical areas and the thalamus." This observation of the apparently uniform and nearly universal innervation pattern of LC-NE cells is part of a broader belief in the second half of the 20th century that the LC is homogenous in the distribution of outgoing axonal pathways and that it impacts brain state by global, synchronized activation. In the first two decades of the 21st century, this assumption has been proved to be incorrect and is one of the several aspects in which the view of NE anatomy and function has increased in nuance in recent years and indeed remains to be further interrogated.

The understanding of subregional specificity within LC efferent groups increased from the 1970s until the early 2010s,[24,25] leading to the emergence of a modular view of LC architecture from the 2010s to today. New techniques like viral-genetic tracing[21] and RNA barcoding[26] have allowed more recent studies to combine whole-brain scope with precise

targeting of subpopulations of NE cells. Even so, there remain several key areas of disputed NE innervation, notably the striatum, which contains adrenergic receptors[27–31] and has documented noradrenergic transmission,[32,33] but has frequently been reported to lack axonal innervation from NE cell groups.[34] Furthermore, a comprehensive picture of all efferent outputs and their densities is still missing. These questions create a compelling case for further studies harnessing modern technologies to elucidate a complete map of NE axonal innervation.

1.5 Genetic background

The canonical view equates NE neuromodulation with cells in the LC, considering LC to be the only source of ascending NE projections. However, a substantial population of NE cells with broad ascending projections were recently isolated outside of LC.[3] This group of cells is derived from a developmental lineage that is distinct from LC-NE cells. While LC-NE cells are derived from the first rhombomere (r1) of the developing brain, the largest population of NE cells outside of the LC descends from rhombomere 4 (r4). Rhombomeric interactions have been shown to play a role in development of vestibular functions,[35,36] pointing to a functional divergence in LC and non-LC NE cells. Furthermore, initial investigations have shown structural differences in the projection patterns between these populations, with non-LC cells favoring subcortical regions and cerebellum and LC-NE cells sending strong projections to cerebral cortex in addition to subcortical and cerebellar regions.[3] These investigations have not been able to quantitatively compare projection strength by target region or comprehensively map all outputs definitively.

1.6 Physiology & behavior

Upon release, NE acts on several G-protein Coupled Receptor adrenergic receptors to effect varied outcomes upon post-synaptic cells. Alpha-1 receptors decrease resting potassium conductance, directly depolarizing interneurons. Alpha-2 receptors increase network firing by closing HCN channels but decrease neurotransmitter release by blocking Cav2.2 channels.[37] This effect may be inhibited by Alpha-1 binding. Both alpha adrenergic receptors inhibit the production of cyclic AMP (cAMP)[38,39], while beta adrenergic receptors increase cAMP production[40]. Beta adrenergic receptors can increase action potential (AP) frequency by inhibiting calcium activated potassium channels and thereby suppressing after-hyperpolarization[37]. They also promote GluR1 receptor membrane insertion, increasing excitability, while contrastingly increasing GABA-AR currents, increasing sensitivity to inhibitory currents.[37]

NE-producing cells express alpha-2 receptors, which mediate a local inhibitory effect upon firing. NE release near the soma location results in auto-inhibition which regulates the transition between the two major modes of firing activity—phasic and tonic release. Tonic NE release is drawn-out, low-frequency, low level activity that regulates changes in brain state over long time scales, while phasic release is higher in both frequency and intensity and is associated with moments of task engagement.

The distinction between these two active states is central to the understanding of NE's functions throughout the brain. Many researchers support a model in which the balance of tonic and phasic activation drives attention in mammals, with low tonic NE activity producing an inattentive state, moderate tonic activity combined with phasic activation producing a task engaged state, and high tonic activity without phasic activation producing an overactive and

distractible state.[41] Figure 1.4 illustrates this principle, known as the Yerkes-Dodson relationship, represented by an inverted U shape.

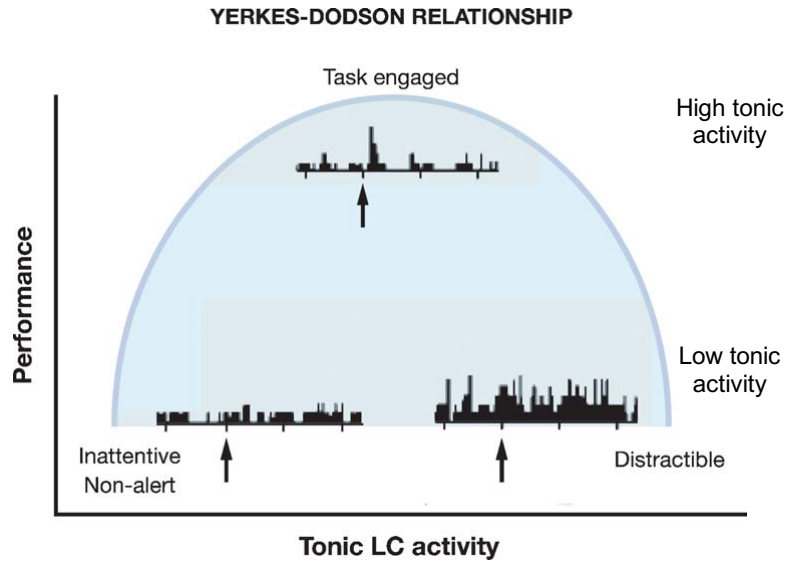

Figure 1.4:[41] The Yerkes-Dodson relationship postulates that tonic LC-NE activity mediates the transition between the three brain states

By exerting this kind of variable influence throughout the many projection areas that receive their input, LC-NE cells are able to effect dramatic changes in behavior ranging from cognitive to motor to memory functions. LC was long considered to be functionally homogenous, modulating brain state by collective activation and widespread NE release,[42] but it has recently become apparent that LC cells co-activate in a modular pattern that is correlated with projection profile, effecting disparate impacts on their particular downstream targets asynchronously.[43,44]

Another important way in which LC cells demonstrate cell-type specific downstream effects is through the co-release of other neurotransmitters. Evidence has primarily demonstrated co-release of DA, but EPI, galanin, and other neuropeptides have been shown to be co-released with NE as well.[45–47] This phenomenon poses another compelling challenge for future study, as the evidence documenting co-release from NE terminals in the past has relied upon candidate regions and temporally limited techniques like micro-dialysis and has not directly demonstrated the reality or mechanism of co-release from the same terminals. Furthermore, it is not known

whether the chemical contents of NE terminals vary by efferent region. More so, the chemical content of terminal release sites remains to be mapped onto the emerging modular architecture of NE soma distribution both within and outside the LC.

1.7 Summary

Each of the major areas outlined above demonstrates the impressive body of work that has been devoted to the study of LC and NE structure and function. Each of these areas also reveals that the most compelling questions that remain to be answered at this moment relate to the cell type diversity and modular architecture of NE cell groups. The experimental design and results documented in the following chapters aim to address some of these most pressing questions, including efforts towards delineating the whole brain distribution of NE cells and comparing that distribution between genetically defined cell types.

Chapter 2: Results

Introduction

In order to address questions about network structure, modular architecture, and cell type diversity in the NE system that I outlined in the previous chapter, I have endeavored to comprehensively map all NE projections from LC and non-LC cells. Firstly, I used the genetic strategy designed by our collaborators in Patricia Jensen's lab at the National Institutes of Health (NIH)[48] as well as stereotaxic viral injection to isolate LC and non-LC. Next, I verified the fidelity of each strategy labeling outgoing axons from each cell group. Collaborators in Zhuhao Wu's lab at Mount Sinai School of Medicine collected images of the resulting fluorescence in the whole brain, and I worked towards establishing methods of analyzing the resulting images and recording NE release at target sites using a fluorescent NE sensor.

The preliminary data support the established perspective of broad bi-hemispheric NE innervation[41] (Fig 2.2). The completed analysis of this dataset has the potential to resolve controversies about areas like the hippocampus[22,49] and striatum[27,34] that have received conflicting reports from previous studies about innervation by NE fibers, and will conclusively reveal the differences in projection pattern between LC and non-LC NE cells.

In the future, the experiment and analysis pipeline laid out in what follows can be used for sparse retrograde labeling to determine soma locations for particular innervated targets to test the hypothesis that NE cells are modularly organized into efferent groups. Future experiments may also use the GRAB-NE sensor employed here[50] in combination with other extracellular sensors (ie GRAB-DA[51]) to test for co-release of other neurotransmitters from NE terminals. Lastly, while an initial attempt was made in this study to further sub-divide NE cells beyond LC vs non-LC with small, hyper-precise stereotactic injections, further studies can build upon the

method outlined below or harness genetic differences resulting from rhombomeric origin of NE cell groups to further investigate differences in anatomy and function between them.

2.1 Characterization of NE cell type labeling strategies

The initial goal of this study was (a) to label all NE cells comprehensively, and (b) to label LC and non-LC cells selectively. I tested both viral and transgenic methods to accomplish each of these goals.

Early on, transgenic labeling strategies were emphasized because they are more likely to label *all* NE cells regardless of soma location. However, initial results from previous characterization experiments in the lab revealed that *Dbh-Cre,*[52] the transgenic line inducing Cre expression in all *Dbh* (and therefore all NE) cells, has some leaky expression in cortical layer 5 as revealed by fluorescent tagging by the Cre reporter line *Ai9.*[53] I verified these results with my own characterization of the *Dbh-Cre;Ai9* cross (Fig 2.1 A). I also observed non-LC cells labeled

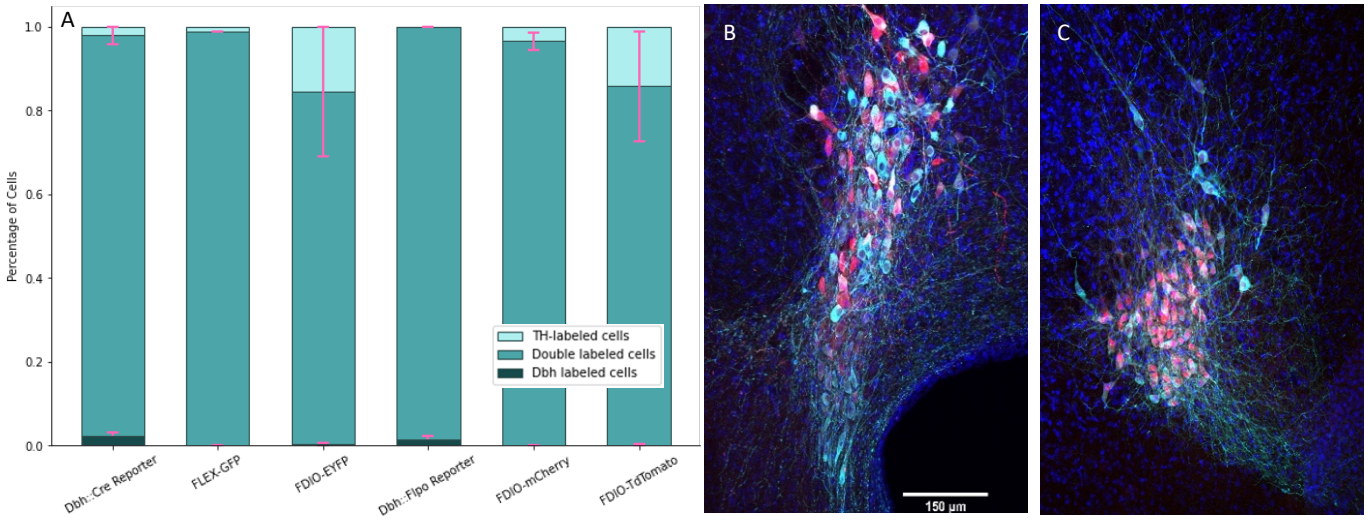

Figure 2.1 Characterization shows efficacy of *Dbh*-defined NE cell population through viral and transgenic labeling strategies. (A) Light teal bars represent cells confirmed to be *Dbh*/NE-positive using TH immunostaining, dark teal bars represent cells labeled by each strategy listed on the x axis, and their overlap in medium teal represents the proportion of counted cells that were both flagged by the experimental label and confirmed by TH immunostain. (B) FLEX-virus labeled cells in LC of Dbh::Cre animal (cyan), anti-TH immunostained cells (red) (C) Transgenically labeled *Dbh-Cre* cells (cyan), anti-TH (red) as in (B)

in layers 5 and 6 of cortex (data not shown). I validated the cell type identity of the ectopic label and the pons NE somas using a TH antibody stain. Note that in and around LC there are no DA-producing cells, so TH serves as the field-accepted marker of NE cells in this area. I did conduct some preliminary tests to verify that this is the case using a DA transporter (DAT) stain in LC, but the antibody did not label effectively and the results were inconclusive.

Once I was sure that the *Dbh-Cre* transgenic reporter would not be an effective strategy for my aims, I pursued two parallel alternative strategies. Firstly, I began targeting LC-NE cells with a Cre-dependent (FLEX)[54] virus (AAV2-FLEX-CAG-GFP) to assess both the selectivity of the viral label and my ability to cover all NE cells within and/or around LC. I applied the same TH immunostain validation procedure and found that 99% of the cells labeled by the FLEX-GFP virus were verified by the TH stain and only 0.01% of TH-verified NE cells in LC were not labeled by the viral injections.

I still wanted to pursue a transgenic strategy, however, that could more conclusively label all NE cells even outside of LC. To this end, I secured and began testing several Flp-dependent (FDIO) viruses hoping that the Flp expression in transgenic mice (B6.129S7(FVB)-*Dbh*$^{tm1.1(flpo)Pjen}$/J[3]) would be more faithful than Cre mice. I tested three FDIO viruses and found that both red viruses (FDIO-TdTomato[55] and FDIO-mCherry) had comparable efficacy to the FLEX-GFP virus, but the FDIO-EYFP virus displayed some ectopic expression. Overall, I had success with Cre-dependent viruses and red Flp-dependent ones. In the future, the Flp-reporter line *Ai65F* should be further characterized and efforts extended to produce or secure a more robust green-tagged Flp-dependent virus for two-color labeling of multiple cells groups in a single brain.

2.2 Comprehensive LC-NE whole brain images

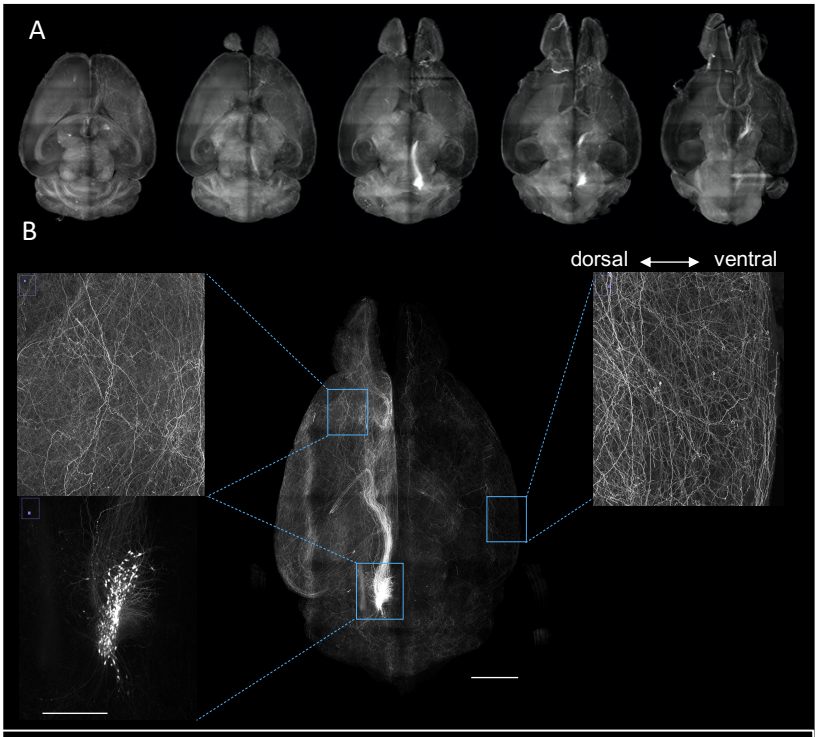

Figure 2.2 Whole brain images show LC injection site and NE fibers throughout the brain. Enhanced signal using GFP antibody (A) Consecutive horizontal digital slices (maximum intensity over 600 um) including midbrain and LC (B) Central slice with injection site and ipsilateral and contralateral target area insets. Scale: 2mm whole brain, 1mm insets

While characterization of Flp-dependent labeling strategies was underway, I initiated a first round of whole brain imaging using FLEX-GFP viral injections in LC. With the help of Drs. Zhuhao Wu and Wei Wang, we processed seven brains. I injected 3 male and 4 female mice with FLEX-tdTomato or FLEX-GFP in either right or left hemisphere LC. The Wu lab cleared the brains and amplified the fluorescence signal using an iDISCO-based clearing and immuno-amplification method.[56] We tried red (FLEX-TdTomato) and green (FLEX-GFP) viruses and found that the FLEX-GFP provided the best signal-to-noise ratio with the antibody enhancement. Figure 2.2 shows an overview of the resulting images taken by the Wu lab on a custom light sheet microscope. Resulting images capture fluorescence throughout the 16-bit dynamic range at 1.866 µm/pixel. Image assembly and stitching of tiles in each z-plane were also performed by the Wu lab. Insets show injection site and traveling fibers on the ipsi- and contra-lateral sides.

We also tried a double reporter strategy developed by the Jensen lab[57] for labeling all LC and non-LC NE cells transgenically. This was accomplished by a cross of *En1-Cre* with *Dbh-Flpo* and the subtractive double reporter line *RC::FLTG*. In this construct, the universal CAG promoter activates *RC::FLTG* in all cells, as illustrated in Figure 2.3 (adapted from Plummer *et al* 2015) but is followed by a STOP sequence that is only inverted in the presence of Flpo—in this schema, only in norepinephrine cells marked by *Dbh-Flpo*. For NE cells, the following TdTomato STOP is expressed, unless, Cre is also present, inverting it. These animals had Cre is in all *En1* cells, which include the cerebellum and parts of the midbrain, only overlapping with *Dbh* in the LC itself. In this way, LC cells were allowed to express the final eGFP sequence, finally resulting in GFP expression in LC-NE cells and TdTomato expression in all other NE cells. Unfortunately, the non-LC cell group in these animals was not clearly labeled and the axons were not easily distinguished from background. For this reason, we began pursuing finely targeted viral injections in order to infect only subgroups of NE cells with each injection.

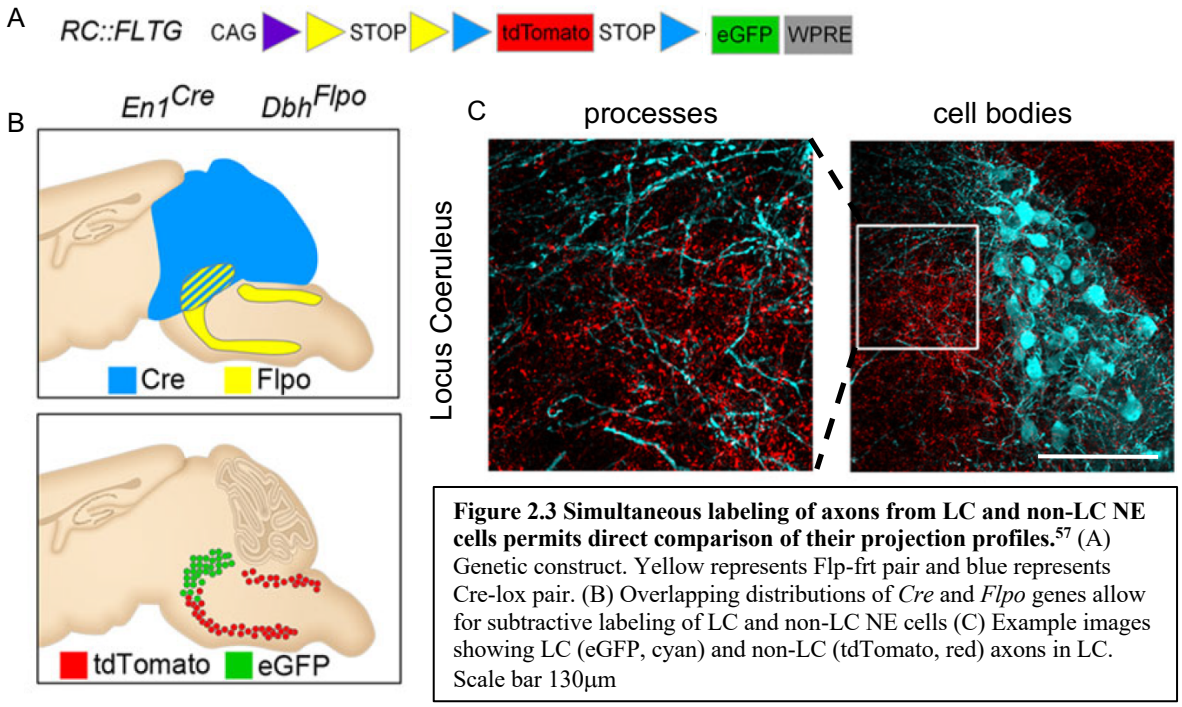

Figure 2.3 Simultaneous labeling of axons from LC and non-LC NE cells permits direct comparison of their projection profiles.[57] (A) Genetic construct. Yellow represents Flp-frt pair and blue represents Cre-lox pair. (B) Overlapping distributions of *Cre* and *Flpo* genes allow for subtractive labeling of LC and non-LC NE cells (C) Example images showing LC (eGFP, cyan) and non-LC (tdTomato, red) axons in LC. Scale bar 130µm

2.3 Selective targeting of rhombomeric subgroups

Initially, I determined optimum coordinates to target LC-NE cells as consistently and comprehensively as possible. I established these coordinates in my first months of training on stereotactic injection and honed them over dozens of injections following. Compared to the target area size, routine 50nL injections were too large for targeting any sub-populations in the area. However, it was hard to know exactly how large the viral spread was since the FLEX virus only labels NE cells, which are tightly clustered spatially.

For this reason, I began target practice with fluorescent retro beads which reveal the location of the injection center regardless of the types of cells present. These also provided an additional advantage since I was able to forgo the weeks-long viral incubation period, slicing and imaging the bead-injected brains on the same or the following day after injection. I used the Paxinos Mouse Brain Atlas (PMBA) and the stereotactic coordinates of my previously successful LC injections to determine candidate coordinates for the other NE structures in the midbrain.

In total, I performed fourteen rounds of stereotactic injections aimed at isolating LC from non-LC NE structures. I tried pressure injections ranging from 10 to 70 nL in volume and iontophoretic injections using varying currents and charge times. In the end, I used large 70 nL injections in coordinates that were ventral, lateral, and posterior to the LC. This injection strategy allowed me to most consistently infect the largest area of non-LC NE cells without infecting cells in LC proper. Table 2.1 summarizes the ranges I spanned in my viral targeting and the final coordinates I used. Note that I eventually excluded the posterior part of SubCV because the SubCV anterior injection provided partial coverage of the posterior section and because I was not able to separately target the posterior region without infecting LC as well.

Structure	Number of Injections	DV Span	ML Span (absolute val)	AP Span	Final DV	Final ML	Final AP
SubCV anterior	18	4650-5200	978-1250	3700-4489	5000	1250	3700
SubCV posterior	11	5000-6200	800	4650	N/A	N/A	N/A
A1	19	5000-6500	100-1500	6500-6800	5500	900	6800
A2	20	4500-6200	0-900	6600-6800	5000	0	6800
A5	4	5500	0-1100	6000	5500	1100	6000

Table 2.1 Non-LC NE Targeting with Stereotactic injection. This table summarizes the stereotactic injections performed to target non-LC NE structures including the number of injections, the anatomical ranges of those injections, and the final coordinates used. All coordinates given in μm ventral, lateral, and posterior to bregma. SubC: sub-coeruleus ventral part; A1, A2, A5: respective brainstem noradrenergic areas.

2.4 Efforts towards injection site segmentation

In parallel to my efforts under the stereotax, I started creating an analysis pipeline to interrogate NE network structure. For initial tests of the analysis technique, I used Z-projected (2D) confocal images collected during characterization experiments and 3D images produced from brains containing viral injections in central amygdala conducted by my lab-mate Michael Muniak and processed by the Wu lab using the same iDISCO-based amplification and clearing method used in my project. I used the python package Cellpose[58] to recognize and segment cell bodies in the injection center. Cellpose uses a generalist algorithm composed of a convolutional neural network that has been trained on imaging data of a wide variety of cell types. I tested a range of parameters to fine tune the model to my testing image data. The parameters that can be adjusted by user input include: the expected diameter of each cell in pixels, the flow threshold (the threshold of probability that any given shape is a cell, below which non-cell shapes are excluded), and the minimum size allowed for a cell. Note that, due to changes in names and functionality of parameters between consecutive releases of Cellpose and lapses in documentation, I faced some challenges in finding the correct parameter space to segment the cells in my 2D and 3D images.

I first determined a combination of parameters that I expected to work based on my earliest test runs using the original version of Cellpose and 2D slices of the 3D images produced by Drs Muniak and Wu. The updated Cellpose model was not able to recognize cells using these parameters. By iteratively segmenting my images and plotting the resulting cell counts as a function of each parameter (measured against manually counted 'ground truth'), I was able to reach a regime in which the results were reasonable. However, I still struggled to fine-tune the model to the desired accuracy. The best segmentation result was achieved using an older version of the Cellpose code and fine-tuning parameters to LC cells and is illustrated in Figure 2.4. I had reasonable success in this case, but the process remains to be scaled up to 3D images from whole mount experiments.

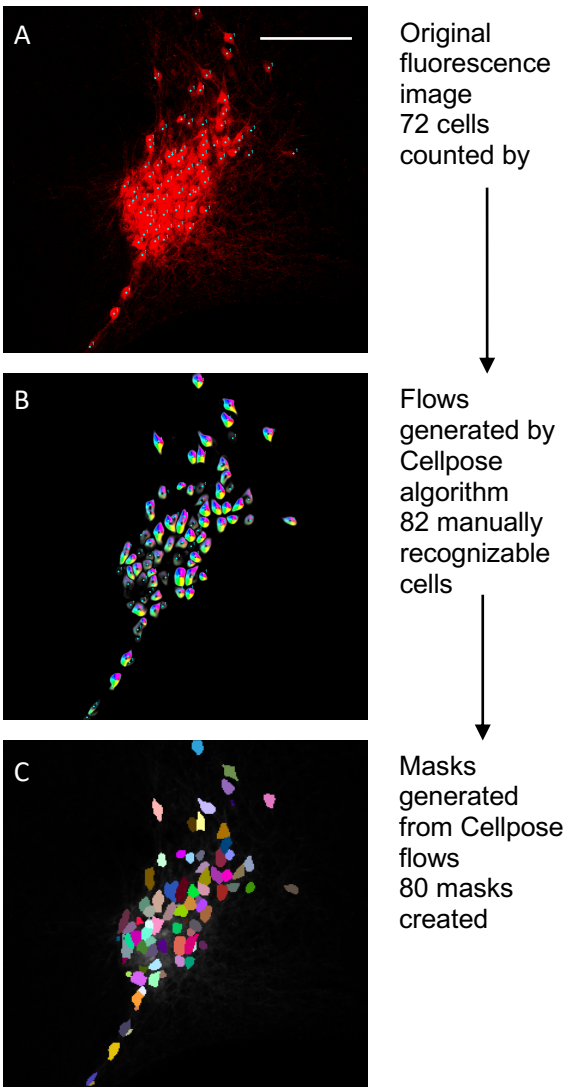

Figure 2.4 Cellpose segmentation pipeline (A) Original fluorescence image of TdTomato labeled NE cells in LC. LUT adjusted to show all cells. Manual cell counting revealed 72 verified cells in the image. Scale bar: 200 μm (B) Results of first step of cellpose analysis on A. Flow lines are calculated before objects are masked based on cell probability. Manually counting flows in the same way as imaged cells reveals 82 cell-like structures. (C) Cellpose masking process identifies 80 cells based on flows.

The next steps, if one is to continue pursuing this analysis, may require re-training the neural network specifically on NE cell imaging data or working with the creators of Cellpose to properly adjust the parameters of the existing model to balance accuracy and sensitivity in this brain region.

2.5 Toward functional readout of NE release

In addition to anatomical imaging and analysis, I further aimed to document NE release at target sites identified by whole brain imaging. I set out to do this using a fluorescent indicator of extracellular NE, GRAB-NE.[50] Furthermore, I hoped that the experimental pipeline established for recording NE release could be expanded in the future to test for co-release of DA from NE terminals using a fluorescent DA sensor in conjunction with GRAB-NE.

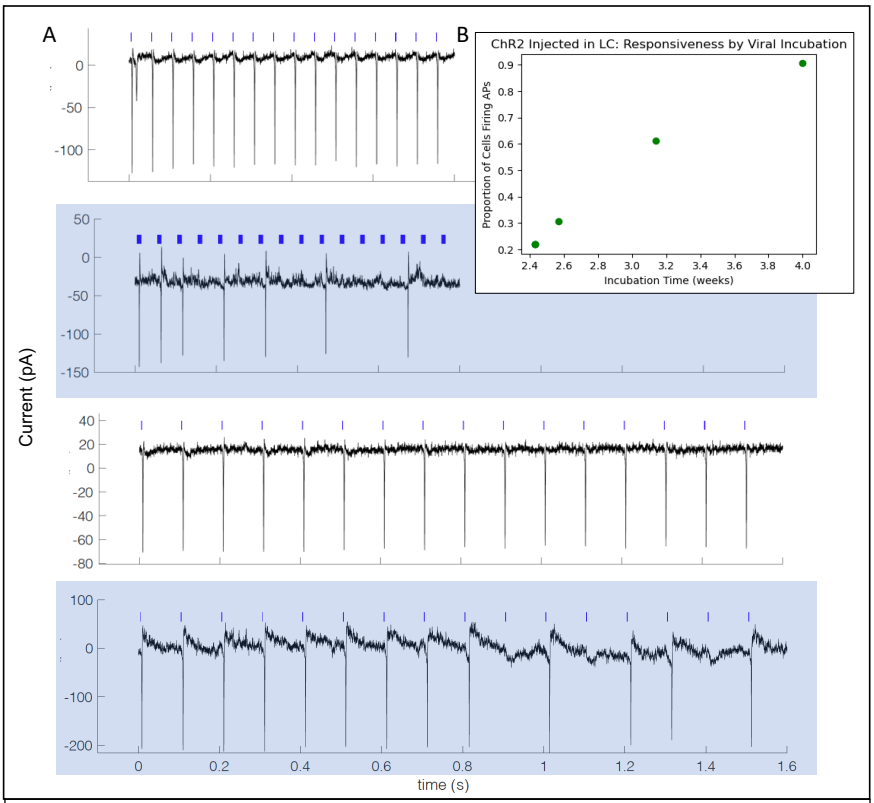

Figure 2.5 Cre-mediated electrophysiological stimulation of LC-NE cells (A) Example cell-attached electrical traces showing activity of a consistently responsive (white background) and a partially responsive (blue background) cell. Top traces show stimulation at 20 Hz, bottom traces show 10 Hz. Recording and analysis by Yang Chen. (B) Proportion of responsive cells by viral incubation time over all trials. From left to right: N=17 cells from 3 animals, 9 cells from 1 animal, 11 cells from 1 animal, 10 cells from 1 animal, respectively.

In order to pursue these goals, I enlisted the help of my lab-mates Yang Chen and Ian Gingerich to verify that we would be able to stimulate NE cells optogenetically. Note that in the final experiment design, we planned for NE stimulation to occur in axonal fibers in live slices taken from terminal field regions, but in pilot experiments we first tested our viral-genetic channelrhodopsin (ChR) paradigm with cell-attached electrophysiological recordings of NE somas in LC.

I injected a Cre-dependent ChR virus (DIO-H134R-EYFP) in LC of *Dbh-Cre* mice, and my lab-mates Yang Chen and Ian Gingerich recorded APs through cell-attached recordings. At four weeks viral incubation time, 90% of recorded cells (N=10 cells from 1 animal) were responsive to optical stimulation. Results are summarized in Figure 2.5.

Once I was confident that this stimulation method could work, I began testing my readout method: the fluorescent GRAB-NE sensor. I injected a virus expressing GRAB-NE2h (AAV9-hsyn-NE2h (h-N05)) in primary motor cortex (M1), a known LC-NE target region, to induce GRAB-NE expression. Then, I bath applied NE at decreasing concentrations in acute slice tissue from M1. I took images of the slice throughout the experiment before and after applying NE and quantified change in fluorescence. I was able to record an increase in fluorescence upon NE application, but the magnitude of increase depended on the concentration of NE applied and the variant of GRAB-NE used (red or green version). Results are summarized in Figure 2.6. Future efforts aimed at combining optogenetic stimulation of LC fibers with fluorescent readout of NE release will likely require a more sensitive measurement of GRAB-NE fluorescence, perhaps with a smaller field of view or a photodiode sensor.

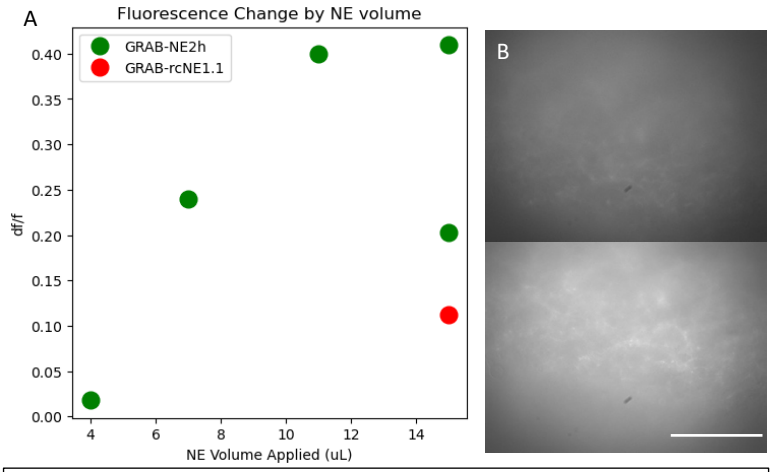

Figure 2.6 GRAB-NE in LC cells senses NE application in M1
(A) Normalized fluorescence change by NE volume applied (uL of 10mM NE). Red shifted sensor in red, original in green (B) Example images show fluorescence change before and after application of 15 uL of 10 mM NE. Scale bar: 50µm

Chapter 3: Materials & Methods

Experimental protocols were conducted according to NIH guidelines for animal research and were approved by the Institutional Animal Care and Use Committee at Oregon Health & Science University. All experiments were carried out in accordance with biosafety level 1 guidelines.

3.1 Materials: transgenic mouse lines, viruses, and antibodies

The materials used for recombinant fluorescent label, NE sensing, optogenetic excitation, and cell type verification are detailed in the following table.

	Tool	Source/reference	Designation
Recombinase mouse lines	*Dbh-Cre*	Jackson Laboratory[52]	B6.Cg-*Dbh*$^{tm3.2(cre)Pjen}$/J
	Dbh-Flpo	Patricia Jensen, NIH[3]	B6.129S7(FVB)-*Dbh*$^{tm1.1(flpo)Pjen}$/J
	En1-Cre	Patricia Jensen, NIH[52]	B6.*En1*$^{tm2(cre)Wrst}$/J
Transgenic reporters	*Ai9*	Jackson Laboratory[53]	B6.Cg-*Gt(ROSA)26Sor*$^{tm9(CAG-tdTomato)Hze}$/J
	Ai65F	Jackson Laboratory[59]	B6.Cg-*Gt(ROSA)26Sor*$^{tm65.2(CAG-tdTomato)Hze}$/J
	RC::FLTG	Patricia Jensen, NIH[3]	B6.Cg-*Gt(ROSA)26Sor*$^{tm1.3(CAG-tdTomato,-EGFP)Pjen}$/J
Viruses	FLEX-GFP	UPenn virus vector core	AAV2-FLEX-CAG-GFP
	FLEX TdTomato	UNC virus vector core	AAV2-FLEX-CAG-TdTomato
	FDIO-TdTomato	Patricia Jensen, NIH[55]	AAV5-fDIO-EF1α-TdTomato
	FDIO-mCherry	Bo Li, Cold Spring Harbor Laboratory	AAV1-fDIO-EF1α-mCherry
	FDIO-EYFP	Bo Li, Cold Spring Harbor Laboratory	AAVdj-fDIO- EF1α-eYFP-wpre
	GRAB-NE2h	Yulong Li, University of Washington[50]	AAV9-hsyn-NE2h (h-N05)
	GRAB-rcNE1.1 (h-rN01)	Yulong Li, University of Washington	AAV9-hsyn- rcNE1.1 (h-rN01)
	DIO-ChR2 (H134R)	Karl Deisseroth, Addgene 20298-AAV5	AAV2-DIO- EF1α-ChR2 (H134R)-EYFP
Primary antibodies	Rabbit anti-TH	Sigma Aldrich AB152	Primary antibody raised in rabbit against tyrosine hydroxylase (TH)
	Mouse anti-NET	MAb Technologies NET05-2	Primary antibody raised in mouse against NE transporter (NET)

	Rat anti-DAT	Abcam ab5990	Primary antibody raised in rat against DA transporter (DAT)
Secondary antibodies	Goat anti-rabbit, Alexa594	Invitrogen A11012	Secondary antibody raised in goat against rabbit, conjugated to Alexa Fluor 594
	Goat anti-rabbit, Alexa488	Invitrogen A11008	Secondary antibody raised in goat against rabbit, conjugated to Alexa Fluor 488
	Goat anti-mouse, Alexa594	Invitrogen A11005	Secondary antibody raised in goat against mouse, conjugated to Alexa Fluor 594
	Goat anti-rat, Alexa488	Invitrogen A11006	Secondary antibody raised in goat against rat, conjugated to Alexa Fluor 488

3.2 Stereotactic injections

For anatomical tracing experiments, stereotactic injections were performed on mice of the strains listed above on postnatal day (P) 42 ± 2 days. 10-75 nL of virus was injected by pressure injector or iontophoretic injection. For optogenetic and extracellular NE sensing experiments, mice were injected on P25± 2 days. For all experiments, alignment in the medial/lateral plane was centered at lambda. Otherwise, injections were performed following the procedure outlined in Hunnicutt et al, 2014.[60]

3.3 Tissue preparation & immunohistochemistry

Animals were euthanized 21± 2 days following surgery by exsanguination and decapitation. Animals were perfused transcardially with 50 mL of filtered 7.4 pH phosphate buffered saline (fPBS) at 20°C, followed by 50 mL of ice cold 4% paraformaldehyde in phosphate buffer solution (PFA), and 50 mL more fPBS. Brains were immediately dissected and soaked in 4% PFA for 12-16 hours at 4°C on a gyrator, then washed in 20°C PBS 3 times for 1 hour each.

Tissue was sliced in the horizontal plane on a Leica 1200S vibratome at 20°C in PBS. 100 μm slices were used for histology and 50 μm for immunohistochemistry. All tissue was stored in fPBS with 0.02% sodium azide or mounted on glass microscope slides in Aqua-Poly/Mount.

Immunohistochemical straining was performed on free floating slices in wells containing a block solution consisting of 2% normal goat serum, 0.2% Triton x-100, and 0.02% sodium azide in fPBS. Slices soaked in block solution on a shaker for at least 30 minutes at 20°C before application of primary antibody (see materials table above) in block solution at 1:500, 1:1000, and 1:200 concentration for anti-TH, anti-NET, and anti-DAT, respectively. Primary antibody was applied for 12-16 hours at 4°C. Tissue was then washed in fPBS 4 times at 20°C before application of secondary antibody in block solution at manufacturer-recommended concentrations. Secondary antibody incubation lasted at least 2 hours and was followed by a 10 minute wash in fPBS with 20 mM Hoescht 33342 nuclear stain at 1:5000 concentration. 3 more fPBS washes of at least 10 minutes each followed before tissue was mounted on slides and imaged.

3.4 Imaging

For stereotactic targeting, images were collected on a Zeiss Axio Zoom.V16 microscope at 9x magnification. For characterization of labeling strategies, images were collected using a Zeiss LSM 980 with Airyscan 2 confocal microscope under a 10x magnification air objective. Whole brain images were collected by Zhuhao Wu and Wei Wang at MountSinai School of Medicine using a custom light sheet microscope.

3.5 Physiology

For optogenetic and extracellular NE sensing experiments, animals were euthanized 17-28 days and 7-13 weeks after injection, respectively. In all cases, brains were extracted, sliced, and prepared as in Kissawaa et al., 2021.[61] After sliced tissue rested for at least 40 minutes at 35°C, cell attached recordings or imaging were conducted in a carbogenated artificial cerebral spinal fluid (ACSF) bath at 20°C. 10mM NE in ACSF was applied directly into the bath at volumes listed in Chapter 2. Recordings were performed by Mao lab student Yang Chen.

3.6 Analysis

For characterization experiments, cells were manually counted using the built-in ImageJ plugin.[62] Cells were excluded if they could not be conclusively labeled as present or absent in any single fluorescent channel. All bar and scatter plot data was analyzed using NumPy[63] and Pandas[64] and plotted using Matplotlib.[65] Optogenetic traces were analyzed by Mao lab student Yang Chen using custom Matlab scripts.

Chapter 4: Discussion

The experiments laid out in the previous chapters have been designed toward producing a whole brain NE connectome and whole-brain maps of biologically significant NE sub-populations. The efforts I've achieved along with my colleagues mentioned above towards those ends include: labeling NE cells from LC and non-LC groups, characterizing the efficacy of the viral and genetic labeling strategies employed, producing whole brain images of LC-only axonal projections, as well as initial efforts toward analyzing the whole brain imaging data and measuring NE release at target sites. For each of these components of my project, I will summarize the methodological innovations employed, the significance of the realized or intended results, and any limitations I faced, along with recommended future steps.

4.1 Characterization of NE cell type labeling strategies

Documenting the accuracy and completeness of the viral and genetic methods that were used for labeling NE cells is essential in order to trust that any conclusions drawn from the resulting connectome datasets are trustworthy. Several of the strategies used have been developed recently by collaborating labs, including the Flp-dependent viruses from Bo Li and the double reporter mouse line from Patricia Jensen ([3], personal communication, reagents not published). These tools are highly innovative contributions to the field. Our application of these tools at a large scale represents a key step in the advancement of each of these tools. Reproducing the in-house characterization that the developing labs conducted of these technologies bolsters their reliability in the field and helps grow them as technologies that can advance many kinds of cell-type specific research programs.

The characterization process confirmed that many of the strategies employed were robust and accurate, but it also revealed some technological roadblocks associated with several of the tools I tested. Firstly, the Cre-reporter *Ai9*[53] confirmed that the *Dbh-Cre* line[66] includes ectopic label in cortical layers 5 an d 6, disqualifying it from use for whole brain tracing. Because of this, I transitioned to the orthogonal FLP-FRT system in hopes of achieving complete and selective transgenic label of all NE cells. I tested three FLP-dependent viruses, but the FLP reporter *Ai65F*[59] remains to be characterized in my hands. In testing the FDIO (FLP-dependent) viruses, I found that the EYFP-tagged virus failed to label a satisfactory proportion of NE cells in LC, meaning that only red FLP-dependent viruses are available for use. Since there are not yet any other differentiably-colored FLP-dependent AAV viruses available, our ability to use a two-color system to compare cell populations in the same brain was inhibited. To solve these problems, we will need to work with collaborators more to develop and test new tools to (a) comprehensively label all NE cells with a genetic reporter and (b) differentiably label subpopulations using non-overlapping fluorescent tags.

4.2 Comprehensive LC-NE whole brain images

This dataset represents the first time the LC-NE system has been imaged at the whole brain scale at this sensitivity and resolution. We were able to achieve this because of the innovations in virus and mouse genetics outlined above along with the tissue clearing, fluorescent immuno-enhancement, and light sheet imaging conducted by collaborators in the Wu lab at MountSinai School of Medicine, pioneers of the iDISCO+ method.[56] Furthermore, the work I did targeting LC and non-LC substructures using precise stereotactic targeting methods

builds upon years of expertise developed in the Mao lab in previous connectome projects mapping thalamic and striatal connections.[60,67]

Combining these areas of technical expertise with the pressing biological questions detailed in Chapter 1 represents a further innovation and a valuable contribution to the field of whole brain connectomics. The resulting images are unique in scale and detail, and when the analysis pipeline is completed, they can provide key insights into the LC-NE signaling network. The work detailed here also represents a pathway toward future discovery as the same methods can be applied to other cell groups including, but not limited to, NE subgroups.

Still, there are limitations to be considered with the current dataset. Even though I have verified that the virus used for the whole brain LC-NE images (FLEX-GFP) infects NE cells at the injection site with great accuracy and completeness, we still need to verify that all LC is covered by the injections in these particular brains and that the sub-coeruleus, a neighboring non-LC region containing NE cells, is not infected. In the future, a transgenic labeling method should be applied to this question to ensure comprehensive label. Further, a subtractive labeling technique like the one pioneered using *RC::FLTG* would provide the most reliable results by genetically isolating LC-NE cells and removing any variability in the stereotactic injection process.

4.3 Selective targeting of rhombomeric subgroups

My efforts toward virally targeting subgroups of NE cells added to the existing capability of stereotactic injections in the Mao lab by targeting non-LC structures in very deep and very posterior regions that we have not attempted to infect before. This set of experiments also documented the limitations of stereotactic injections for precise targeting of tight anatomically-defined groups of cells. I was not able to infect the deepest NE cells in noradrenergic area 7 (A7) because they are located too ventrally in the brain stem. Additionally, I was not able to be totally selective between rhombomeric subgroups because the ontologically defined NE regions are located so closely together and because rhombemberic distributions do not entirely follow the ontological categories established by anatomists, but rather are intermixed throughout several regions.[3] Genetic reporters or genetically defined Cre/Flp-prohibitive viruses will likely be necessary to accomplish selective labeling of rhombomeric groups. These data support this conclusion and can inform future efforts to these ends.

4.4 Efforts towards alignment with quantitative assessment and injection site segmentation

Efforts toward digitally segmenting the cells labeled in each whole brain are significant as this is the first step in drawing conclusions about network density and classifying cell groups by projection architecture. We have to know where and how many cells there are and register them into a digital space overlaid with an ontology of brain regions before we draw meaningful conclusions about their axonal projections. Furthermore, the development of the analysis pipeline itself is a worthwhile contribution to a growing field. Whole brain connectomics are emerging as an important frontier in systems neuroscience, and finding reliable ways to analyze imaging datasets to produce connectomes is an important key to unlocking network-level

insights. Several research groups have made advances in this area,[56,68,69] and this project can add to this growing body of work toward collectively producing the best system for analysis. Additionally, this is the first time Cellpose has been used in conjunction with a 3D whole brain projectome at this scale. Extending the use of a publicly available general-purpose algorithm to new types of datasets is an important advancement of this technology for the field.

The complete whole brain analysis including alignment/registration to atlases, soma and axon segmentation, and network analysis are still a long way off. Namely, Cellpose has not been as successful as we would like in segmenting soma bodies. What I have accomplished in the troubleshooting of these early stages can be built upon in future research. Next steps will be to work with the creators to get a better handle on the parameters, retrain the model on our own images, or write new code to accomplish the analysis.

An overview of the intended image analysis pipeline is provided in Figure 4.1.

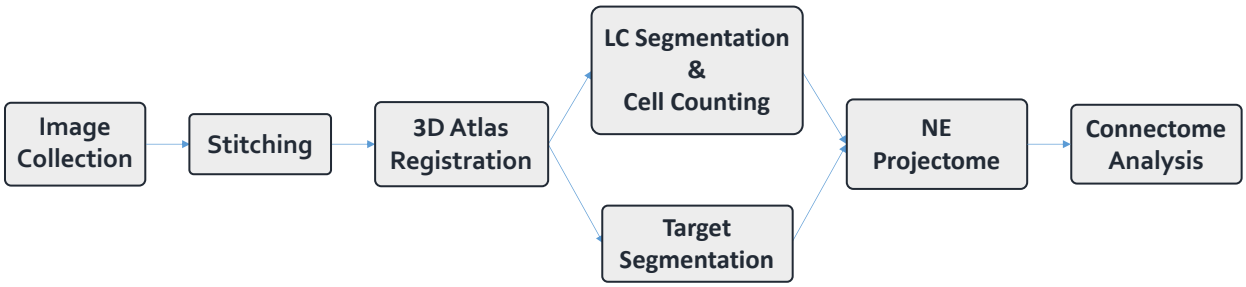

Figure 4.1 Proposed whole brain connectome analysis pipeline

4.5 Toward functional readout of NE release

When fluorescent sensing of NE release at target sites is implemented, it will yield long-awaited conclusions about the functional element of NE signaling. For instance, is NE actually released in all the regions that have terminals from NE axons? What about regions like striatum, where there are adrenergic receptors but many have documented no NE terminals?[27,34] Additionally, this method can be used in conjunction with other sensors, like GRAB-DA[51] to measure co-release of NE with other transmitters purported to be released by NE cells. GRAB-NE is a promising new technology that has only undergone initial testing so far. The body of data documenting its usefulness can be expanded by this work, and combining it with extensive anatomical data represents a meaningful new innovation.

The current imaging setup used in the experiments documented here, however, cannot measure physiological levels of NE, so sensitivity will need to be increased either by zooming in on cells (or analyzing regions of interest instead of the entire field of view) or installing a photodiode for increased sensitivity over the camera currently being used. Lastly, a robust red ChR or red-tagged NE sensor will be necessary to effectively combine optical stimulation with readout of extracellular NE.

4.5 Conclusions

In conclusion, throughout the work detailed in this document, I gained detailed knowledge about the field of NE research and charted a course to answer some of the pressing and accessible questions. With the help of collaborators within and beyond the Mao lab, I took several major steps toward answering these and laid out a plan for future research to continue.

References

1. Loughlin, S. E., Foote, S. L. & Grzanna, R. Efferent projections of nucleus locus coeruleus: Morphologic subpopulations have different efferent targets. *Neuroscience* **18**, 307–319 (1986).
2. Moore, R. Y. & Bloom, F. E. Central Catecholamine Neuron Systems: Anatomy and Physiology of the Norepinephrine and Epinephrine Systems. *Annu. Rev. Neurosci.* **2**, 113–168 (1979).
3. Robertson, S. D., Plummer, N. W., de Marchena, J. & Jensen, P. Developmental origins of central norepinephrine neuron diversity. *Nat Neurosci* **16**, 1016–1023 (2013).
4. Lindvall, O., Björklund, A., Nobin, A. & Stenevi, U. The adrenergic innervation of the rat thalamus as revealed by the glyoxylic acid fluorescence method. *Journal of Comparative Neurology* **154**, 317–347 (1974).
5. Schwarz, L. A. & Luo, L. Organization of the Locus Coeruleus-Norepinephrine System. *Current Biology* **25**, R1051–R1056 (2015).
6. Poe, G. R. *et al.* Locus coeruleus: a new look at the blue spot. *Nature Reviews Neuroscience* **21**, 644–659 (2020).
7. Paravati, S., Rosani, A. & Warrington, S. J. Physiology, Catecholamines. in *StatPearls* (StatPearls Publishing, 2022).
8. Oliver, G. & Schäfer, E. A. The Physiological Effects of Extracts of the Suprarenal Capsules. *J Physiol* **18**, 230–276 (1895).
9. Stanford, S. C. & Heal, D. J. Catecholamines: Knowledge and understanding in the 1960s, now, and in the future. *Brain and Neuroscience Advances* **3**, 2398212818810682 (2019).
10. Wassall, R. D., Teramoto, N. & Cunnane, T. C. Noradrenaline. in *Encyclopedia of Neuroscience* (ed. Squire, L. R.) 1221–1230 (Academic Press, 2009). doi:10.1016/B978-008045046-9.00681-1.
11. Russell, G. V. The nucleus locus coeruleus (dorsolateralis tegmenti). *Tex Rep Biol Med* **13**, 939–988 (1955).

12. Snider, R. S. A cerebellar-ceruleus pathway. *Brain Res* **88**, 59–63 (1975).

13. Scheibel, M. E. & Scheibel, A. B. The Brain Stem Reticular Core—An Integrative Matrix. in *Systems Theory and Biology* (ed. Mesarović, M. D.) 261–285 (Springer, 1968). doi:10.1007/978-3-642-88343-9_13.

14. Shimizu, N., Onishi, S., Toyama, M. & Maeda, T. Demonstration by degeneration silver method of the ascending projection from the locus ceruleus. *Exp Brain Res* **20**, 181–192 (1974).

15. Maeda, T. & Shimizu, N. Projections ascendantes du locus coeruleus et d'autres neurones aminergiques pontiques au niveau du prosencéphale du rat. *Brain Research* **36**, 19–35 (1972).

16. Cedarbaum, J. M. & Aghajanian, G. K. Afferent projections to the rat locus coeruleus as determined by a retrograde tracing technique. *J. Comp. Neurol.* **178**, 1–15 (1978).

17. Krettek, J. E. & Price, J. L. Amygdaloid projections to subcortical structures within the basal forebrain and brainstem in the rat and cat. *J. Comp. Neurol.* **178**, 225–253 (1978).

18. Post, S. & Mai, J. K. Contribution to the amygdaloid projection field in the rat. A quantitative autoradiographic study. *J Hirnforsch* **21**, 199–225 (1980).

19. Clavier, R. M. Afferent projections to the self-stimulation regions of the dorsal pons, including the locus coeruleus, in the rat as demonstrated by the horseradish peroxidase technique. *Brain Research Bulletin* **4**, 497–504 (1979).

20. Price, J. L. & Amaral, D. G. An autoradiographic study of the projections of the central nucleus of the monkey amygdala. *J Neurosci* **1**, 1242–1259 (1981).

21. Schwarz, L. A. *et al.* Viral-genetic tracing of the input–output organization of a central noradrenaline circuit. *Nature* **524**, 88–92 (2015).

22. Swanson, L. W. & Hartman, B. K. The central adrenergic system. An immunofluorescence study of the location of cell bodies and their efferent connections in the rat utilizing dopamine-beta-hydroxylase as a marker. *J Comp Neurol* **163**, 467–505 (1975).

23. Olson, L. & Fuxe, K. On the projections from the locus coeruleus noradrenaline neurons: The cerebellar innervation. *Brain Research* **28**, 165–171 (1971).

24. Noradrenergic and serotoninergic innervation of cortical, thalamic, and tectal visual structures in old and new world monkeys - Morrison - 1986 - Journal of Comparative Neurology - Wiley Online Library. https://onlinelibrary.wiley.com/doi/abs/10.1002/cne.902430110.

25. The distribution of tyrosine hydroxylase-immunoreactive fibers in primate neocortex is widespread but regionally specific | Journal of Neuroscience. https://www.jneurosci.org/content/7/1/279.

26. Kebschull, J. M. *et al.* High-Throughput Mapping of Single-Neuron Projections by Sequencing of Barcoded RNA. *Neuron* **91**, 975–987 (2016).

27. Meitzen, J., Luoma, J. I., Stern, C. M. & Mermelstein, P. G. β1-adrenergic receptors activate two distinct signaling pathways in striatal neurons. *J Neurochem* **116**, 984–995 (2011).

28. Nicholas, A. P., Pieribone, V. & Hökfelt, T. Distributions of mRNAs for alpha-2 adrenergic receptor subtypes in rat brain: an in situ hybridization study. *J Comp Neurol* **328**, 575–594 (1993).

29. Paschalis, A. *et al.* beta1-Adrenoceptor distribution in the rat brain: an immunohistochemical study. *Neurosci Lett* **458**, 84–88 (2009).

30. Pisani, A. *et al.* Activation of beta1-adrenoceptors excites striatal cholinergic interneurons through a cAMP-dependent, protein kinase-independent pathway. *J Neurosci* **23**, 5272–5282 (2003).

31. Rommelfanger, K. S., Mitrano, D. A., Smith, Y. & Weinshenker, D. Light and electron microscopic localization of alpha-1 adrenergic receptor immunoreactivity in the rat striatum and ventral midbrain. *Neuroscience* **158**, 1530–1540 (2009).

32. Forn, J., Krueger, B. K. & Greengard, P. Adenosine 3',5'-monophosphate content in rat caudate nucleus: demonstration of dopaminergic and adrenergic receptors. *Science* **186**, 1118–1120 (1974).

33. Harris, J. E. Beta adrenergic receptor-mediated adenosine cyclic 3',5'-monophosphate accumulation in the ratcorpus striatum. *Mol Pharmacol* **12**, 546–558 (1976).

34. Berridge, C. W. & Waterhouse, B. D. The locus coeruleus–noradrenergic system: modulation of behavioral state and state-dependent cognitive processes. *Brain Research Reviews* **42**, 33–84 (2003).

35. Glover, J. C. Correlated patterns of neuron differentiation and Hox gene expression in the hindbrain: a comparative analysis. *Brain Research Bulletin* **55**, 683–693 (2001).

36. Borday, C., Coutinho, A., Germon, I., Champagnat, J. & Fortin, G. Pre-/post-otic rhombomeric interactions control the emergence of a fetal-like respiratory rhythm in the mouse embryo. *Journal of Neurobiology* **66**, 1285–1301 (2006).

37. O'Donnell, J., Zeppenfeld, D., McConnell, E., Pena, S. & Nedergaard, M. Norepinephrine: A Neuromodulator That Boosts the Function of Multiple Cell Types to Optimize CNS Performance. *Neurochem Res* **37**, 2496–2512 (2012).

38. Barrett, S., Honbo, N. & Karliner, J. S. Alpha 1-adrenoceptor-mediated inhibition of cellular cAMP accumulation in neonatal rat ventricular myocytes. *Naunyn Schmiedebergs Arch Pharmacol* **347**, 384–393 (1993).

39. Umemura, S., Smyth, D. D. & Pettinger, W. A. Alpha 2-adrenoceptor stimulation and cellular cAMP levels in microdissected rat glomeruli. *Am J Physiol* **250**, F103-108 (1986).

40. Sassone-Corsi, P. The Cyclic AMP Pathway. *Cold Spring Harb Perspect Biol* **4**, a011148 (2012).

41. Aston-Jones, G. & Cohen, J. D. AN INTEGRATIVE THEORY OF LOCUS COERULEUS-NOREPINEPHRINE FUNCTION: Adaptive Gain and Optimal Performance. *Annu. Rev. Neurosci.* **28**, 403–450 (2005).

42. Aston-Jones, G., Ennis, M., Pieribone, V. A., Nickell, W. T. & Shipley, M. T. The brain nucleus locus coeruleus: restricted afferent control of a broad efferent network. *Science* **234**, 734–737 (1986).

43. Totah, N. K. B., Logothetis, N. K. & Eschenko, O. Noradrenergic ensemble-based modulation of cognition over multiple timescales. *Brain Research* **1709**, 50–66 (2019).

44. Noei, S., Zouridis, I. S., Logothetis, N. K., Panzeri, S. & Totah, N. K. Distinct ensembles in the noradrenergic locus coeruleus evoke diverse cortical states. *bioRxiv* 2020.03.30.015354 (2020) doi:10.1101/2020.03.30.015354.

45. Okada, M. & Fukuyama, K. Interaction between Mesocortical and Mesothalamic Catecholaminergic Transmissions Associated with NMDA Receptor in the Locus Coeruleus. *Biomolecules* **10**, (2020).

46. Sonneborn, A. & Greene, R. W. The norepinephrine transporter regulates dopamine-dependent synaptic plasticity in the mouse dorsal hippocampus. *bioRxiv* 793265 (2019) doi:10.1101/793265.

47. Devoto, P. *et al.* Noradrenergic terminals are the primary source of α2-adrenoceptor mediated dopamine release in the medial prefrontal cortex. *Progress in Neuro-Psychopharmacology and Biological Psychiatry* **90**, 97–103 (2019).

48. Robertson, S. D. Developmental origins of central norepinephrine neuron diversity. *nature NEUROSCIENCE* **16**, 10 (2013).

49. Waterhouse, B. D., Lin, C. S., Burne, R. A. & Woodward, D. J. The distribution of neocortical projection neurons in the locus coeruleus. *J Comp Neurol* **217**, 418–431 (1983).

50. Feng, J. *et al.* A Genetically Encoded Fluorescent Sensor for Rapid and Specific In Vivo Detection of Norepinephrine. *Neuron* **102**, 745-761.e8 (2019).

51. Sun, F. *et al.* Next-generation GRAB sensors for monitoring dopaminergic activity in vivo. *Nat Methods* **17**, 1156–1166 (2020).

52. Kimmel, R. A. *et al.* Two lineage boundaries coordinate vertebrate apical ectodermal ridge formation. *Genes Dev* **14**, 1377–1389 (2000).

53. Madisen, L. *et al.* A robust and high-throughput Cre reporting and characterization system for the whole mouse brain. *Nat Neurosci* **13**, 133–140 (2010).

54. Atasoy, D., Aponte, Y., Su, H. H. & Sternson, S. M. A FLEX Switch Targets Channelrhodopsin-2 to Multiple Cell Types for Imaging and Long-Range Circuit Mapping. *J. Neurosci.* **28**, 7025–7030 (2008).

55. Sciolino, N. R. *et al.* Natural locus coeruleus dynamics during feeding. *Sci. Adv.* **8**, eabn9134 (2022).

56. Renier, N. *et al.* iDISCO: A Simple, Rapid Method to Immunolabel Large Tissue Samples for Volume Imaging. *Cell* **159**, 896–910 (2014).

57. Plummer, N. W. *et al.* Expanding the power of recombinase-based labeling to uncover cellular diversity. *Development* **142**, 4385–4393 (2015).

58. Stringer, C., Wang, T., Michaelos, M. & Pachitariu, M. Cellpose: a generalist algorithm for cellular segmentation. *Nat Methods* **18**, 100–106 (2021).

59. Daigle, T. L. *et al.* A Suite of Transgenic Driver and Reporter Mouse Lines with Enhanced Brain-Cell-Type Targeting and Functionality. *Cell* **174**, 465-480.e22 (2018).

60. Hunnicutt, B. J. A comprehensive thalamocortical projection map at the mesoscopic level. *nature NEUROSCIENCE* **17**, 13 (2014).

61. Kissiwaa, S. A. *et al. Synaptotagmin-7 enhances phasic dopamine release*. 2021.10.17.464710 https://www.biorxiv.org/content/10.1101/2021.10.17.464710v2 (2021) doi:10.1101/2021.10.17.464710.

62. Fiji: an open-source platform for biological-image analysis | Nature Methods. https://www.nature.com/articles/nmeth.2019.

63. Harris, C. R. *et al.* Array programming with NumPy. *Nature* **585**, 357–362 (2020).

64. McKinney, W. Data Structures for Statistical Computing in Python. in 56–61 (2010). doi:10.25080/Majora-92bf1922-00a.

65. Hunter, J. D. Matplotlib: A 2D Graphics Environment. *Computing in Science & Engineering* **9**, 90–95 (2007).

66. Tillage, R. P. *et al.* Elimination of galanin synthesis in noradrenergic neurons reduces galanin in select brain areas and promotes active coping behaviors. *Brain Struct Funct* **225**, 785–803 (2020).

67. Hunnicutt, B. J. *et al.* A comprehensive excitatory input map of the striatum reveals novel functional organization. 32.

68. Perens, J. *et al.* An Optimized Mouse Brain Atlas for Automated Mapping and Quantification of Neuronal Activity Using iDISCO+ and Light Sheet Fluorescence Microscopy. *Neuroinform* (2020) doi:10.1007/s12021-020-09490-8.

69. Claudi, F. *et al.* Visualizing anatomically registered data with Brainrender. *eLife* **10**, e65751 (2021).